Since January 2020 Elsevier has created a COVID-19 resource centre with free information in English and Mandarin on the novel coronavirus COVID-19. The COVID-19 resource centre is hosted on Elsevier Connect, the company's public news and information website.

Scientific African 14 (2021) e00970

Contents lists available at ScienceDirect

Scientific African

journal homepage: www.elsevier.com/locate/sciaf

Structure-based virtual screening and molecular dynamics simulation studies to discover new SARS-CoV-2 main protease inhibitors

A. Ibezim[a,*], R.S. Onuku[a], A. Ibezim[b], F. Ntie-Kang[c,d,e,*], N.J. Nwodo[a], M.U. Adikwu[f]

[a] Department of Pharmaceutical and Medicinal Chemistry, Faculty of Pharmaceutical Sciences, University of Nigeria, Nsukka, Nigeria
[b] Information and Communication Technology Unit, University of Nigeria, Nsukka, Nigeria
[c] Department of Chemistry, Faculty of Science, University of Buea, P. O. Box 63, Buea, Cameroon
[d] Institute for Pharmacy, Martin-Luther-Universität Halle-Wittenberg, Kurt-Mothes-Str. 3, 06120 Halle (Saale), Germany
[e] Institute of Botany, Technical University of Dresden, Zellescher Weg 20b, 01217 Dresden, Germany
[f] Department of Pharmaceutical Microbiology and Biopharmaceutics, Faculty of Pharmaceutical Sciences, University of Nigeria, Nsukka, Nigeria

ARTICLE INFO

Article history:
Received 19 March 2021
Revised 13 August 2021
Accepted 9 September 2021

Editor: DR B Gyampoh

Keywords:
Coronavirus
SARS-CoV-2
Main protease inhibitor
Docking
Molecular dynamics
Binding mode prediction

ABSTRACT

Computational methods were used to filter two datasets (> 8,000 compounds) based on two criteria: higher binding affinity for M^{PRO} than cocrystallized inhibitor and binding interactions with M^{PRO} catalytic dyad (Cys145 and His41). After virtual screening involving ranking and reranking, eleven compounds were identified to satisfy these criteria and analysis of their structures revealed an unparallel common features among them which could be critical for their interactions with M^{PRO}. However, only the topmost scoring compound (AV-203: K_i = 0.31 µM) exhibited relatively stable binding interaction during the period of 50 ns MD simulation and thus is a suitable template for drug development.

Introduction

Severe Acute Respiratory Syndrome-CoronaVirus-2 (SARS-CoV-2) is a new strain of coronavirus (COVID-19), first reported from the Wuhan region of China in December 2019 and was declared a pandemic by World Health organisation in March 2020 [1]. As of October 2020, over 40 million cases and 1.1 million deaths have been reported worldwide, mostly in elderly people and children (WHO, 2020). Approximately 95% of world population is at risk of COVID-19 and an estimated 1.7 billion people, comprising 22% of the global population, have underlying health condition that could raise their risk of being seriously ill if infected with COVID-19 [2]. The economic loss and degree of human suffering due to the disease is overwhelming [3]. Even though several scientists are working around the clock, the discovery of COVID-19 drugs and vaccine is still at large [4].

* Corresponding author.
E-mail address: akachukwu.ibezim@unn.edu.ng (A. Ibezim).

https://doi.org/10.1016/j.sciaf.2021.e00970

Among some other critical proteins encoded by SARS-CoV-2 such as nucleocapsid protein [5], Spike (S) protein [6], Envelope (E) protein [7], and Membrane (M) protein [8], the propagation of COVID-19 is reliant on proteases as the SARS-CoV-2 takes over the molecular machinery of host cells of COVID-19 infected persons and produces more copies of RNA through translation into long chains of viral proteins, which are activated when cut into smaller pieces by proteases [9–10]. Two main proteases namely papain-like protease (PLP) and main protease (M^{pro} also known as $3CL^{pro}$) are involved in the cleavage. Hence, viral proteases represent an attractive drug target in the search for COVID-19 drugs and since their crystal structures were deposited in protein databank, a plethora of researchers have targeted them with many classes of small and peptide molecules in search for potential inhibitors [11]. For example, Ghosh et al. [12] screened polyphenols from *Isatis indigotica* root while Peele et al. [13], searched both natural products and US-FDA approved drugs to find potent stable binders of M^{pro}. Kumar et al. [14] and Khan et al. [15], respectively evaluated hydroxyethylamine analogs and marine natural compounds as potent inhibitors against the main protease of SARS-CoV-2 and Ibrahim and his coworkers applied variety of virtual methods to search for novel M^{pro} ligands [16–20]. However, no such studies have been reported for screening antiviral compounds or recognizing the M^{pro} catalytic dyad in selecting potential inhibitors. Therefore, our study is relevant.

In the present work, we employed molecular docking and dynamics strategies to screen a total of ~9000 dataset comprising antiviral compounds and natural products fragments in Enamine database based on two criteria: (1) higher binding affinity than M^{pro} cocrystallized ligand and (2) binding interaction with M^{pro} catalytic dyad - Cys145 and His41. Analysis of binding mode and structure-activity relationship of topscoring compounds were carried out. Finally, molecular dynamic simulations of all the topscoring compounds were made and their behaviours were evaluated based on root mean square deviation (RMSD) of the ligands from the target binding site residues as their complexes evolve.

Materials and method

Selection and preparation of corona virus main protease structure

The three-dimensional structure of corona virus main protease – M^{PRO} – bearing its cocrystallized inhibitor (N3) was selected from protein databank (PDB code: 6LU7). The cocrystallized water molecules and other non-essential particles were removed to retain only the protein-ligand complex. The Protonate 3D procedure implemented in molecular operating environment (MOE) software was used to protonate the complex before energy minimizing it to gradient of 0.001 kcal/mol using the Merck Molecular (MMFF94) force field to eliminate atomic clashes [21–23].

Preparation of the datasets

The modelled structures of two sample datasets comprising compounds with antiviral activity in experimental screening and natural product fragments were downloaded from the Enamine database. To prepare the sample compounds for simulation purposes, the default settings of LigX module in MOE was used.

Docking with MOE

The position occupied by the cocrystallized inhibitor was considered as the binding site of the receptor. Ten conformations of each of the sample compounds were generated and carefully placed into the receptor's binding site by "triangle matcher" module. "London dG" scoring function was used to assign the theoretical free binding energies of the protein-ligand complexes formed before finally being refined by force field.

Docking with AutoDock4.2

The AutoDock4.2 software [24] was used to predict the binding poses and rescore the free energy of interaction for the successful candidates from MOE docking calculations. Rigid-receptor-flexible-ligand docking was carried out by AutoDockTools in which the grid box with 0.375 Å points spacing was centered in the mass center surrounded by the amino acid residues at the receptor binding site. AutoGrid module implemented in AutoDock was used to estimate potential grid maps for the interaction of ligand atom-types. In the docking computations, a total of 250 hybrid GA-LS runs, and at most 2.5 million energy evaluations and 0.27 million generations were performed. To group the clusters, a root mean square deviation tolerance was set at 2.0 Å. Other parameters were kept at default settings during the docking simulations.

Molecular dynamic simulations

Gromacs v4.5.5 and Amber99 force-field were used to perform MD simulation of top docked complexes. Automated Topology Builder (ATB: an online platform) was used to generate the topology and parameter files of ligands [25]. The M^{PRO}-ligand complexes were placed in a cubic box simple point charge (SPC) at 1.0 Å between the box edges and the protein surface and solvated with an explicit water model. Before using steepest descent integrator and conjugate gradient algorithm to energy minimize the system, it was neutralized by the addition of sufficient Na^+ and Cl^- ions. Position restraining force was applied to all non-hydrogen atoms while the solvent molecules and ions were allowed to equilibrate around the solute molecules at 300 k and 1 bar for a simulation time of 50 ns for comparative trajectory analysis [26].

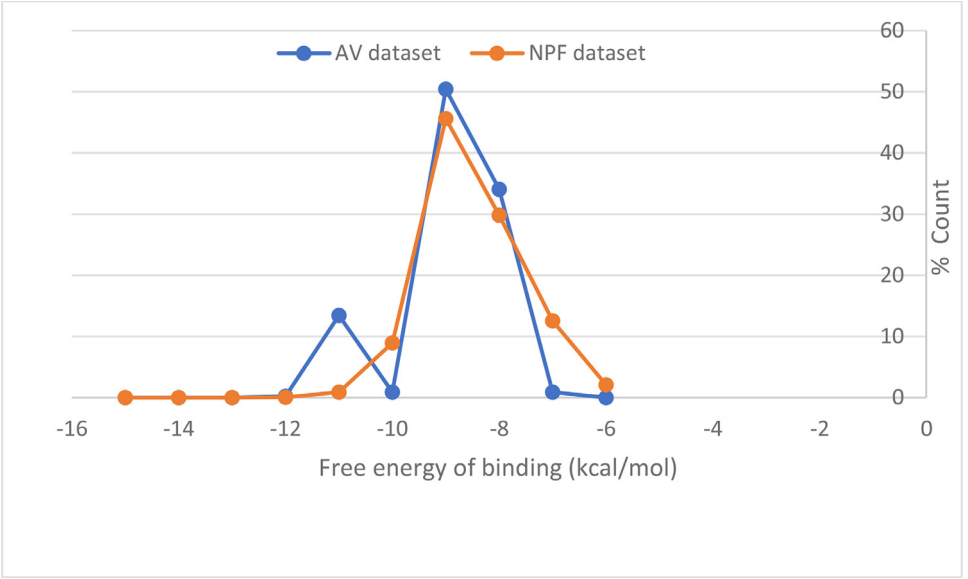

Fig. 1. Distribution of docking scores for the two datasets.

Results and discussion

Natural products have been serving as medicine as far back as time [27–30] and more also, have been guiding the development of several small chemotherapeutic molecules including new chemical entities with antiviral indications [31–32]. A review by Newman and Cragg reported that 4% of antiviral drugs are natural products while 10% are either synthetic molecules with pharmacophore from natural products or natural products mimics [33]. On the other hand, molecules with activity against a particular pathogen is commonly screened in search for an inhibitor for the pathogen's validated drug target [27-29]. Based on the foregoing, we chose to explore the datasets (natural products fragments (NPF) and molecules with experimentally confirmed antiviral effects (AV)) from Enamine library to identify virtual corona virus main protease inhibitors.

Docking and scoring with London dG scoring function

The method of root mean square deviation (rmsd) was used to validate docking protocol. This entails ensuring the protocol produces dock pose of the cocrystallized ligand (N3 – N-[(5-methylisoxazol-3-yl)carbonyl)anyl-L-valyl-N-1-((1R,2Z)−4-(benzyloxy)−4-(benzyloxy)−4-oxo-1-{[(3R)−2-*oxopyrrolidin*-3-*yl*]methyl)but−2-enyl)-L-leucinamide) that compares with X-ray crystallized pose within rmsd of $\leq$ 2.00 Å. After multiple trials, a grid box of 12 $\times$ 12 $\times$ 15 dimension with 0.375 Å spacing centered in -6 $\times$ 11 $\times$ 70 center of mass gave rsmd = 1.82 Å which satisfied the criteria and therefore was used in this study.

Docking and calculations of free binding energy by London dG scoring function implemented in MOE software gave docking score distributions of the two datasets that ranged from −15 to −7 kcal/mol for NPF dataset and −12 to −6 kcal/mol for AV dataset. Both distributions showed a Gaussian curve with a peak value at −9 kcal/mol representing more than 45.60% and 50.43% compounds in NPF and AV datasets respectively (Fig. 1). Two criteria used to select significant candidates were: binding affinity higher than that of N3 and binding interaction with either or both M^{PRO} catalytic residues – Cys145 and His41. It was observed that 60 molecules from NPF library and 184 molecules from AV library had free energy of binding lower than that of N3 (−11.40 kcal/mol) – the cocrystallized inhibitor of M^{PRO}. Additionally, upon visual inspection of binding poses of the 244 molecules (sum of 60 and 184 compounds) it was discovered that only a total of 32 molecules, nicknamed as MOE 32-hits, (8 from NPF and 24 from AV datasets) passed the second requirement and were hence considered for further studies.

AutoDock4.2 docking and rescoring result

Rescoring is commonly practiced because it has been confirmed to produce a better docking conformation of ligand and enhanced theoretical binding free energy. Therefore, AutoDock4.2 software with forcefield-based scoring function was employed to re-rank the MOE 32-hits from virtual screening with MOE. Again, rmsd method was used to validate AutoDock4.2 docking protocol. A grid box points 60 $\times$ 60 $\times$ 60 with 0.375 Å spacing centered on mass center of −10.153 $\times$ 13.266 $\times$ 68.742, which reproduced experimental pose of the cocrystallized inhibitor within 1.94 Å rmsd, was

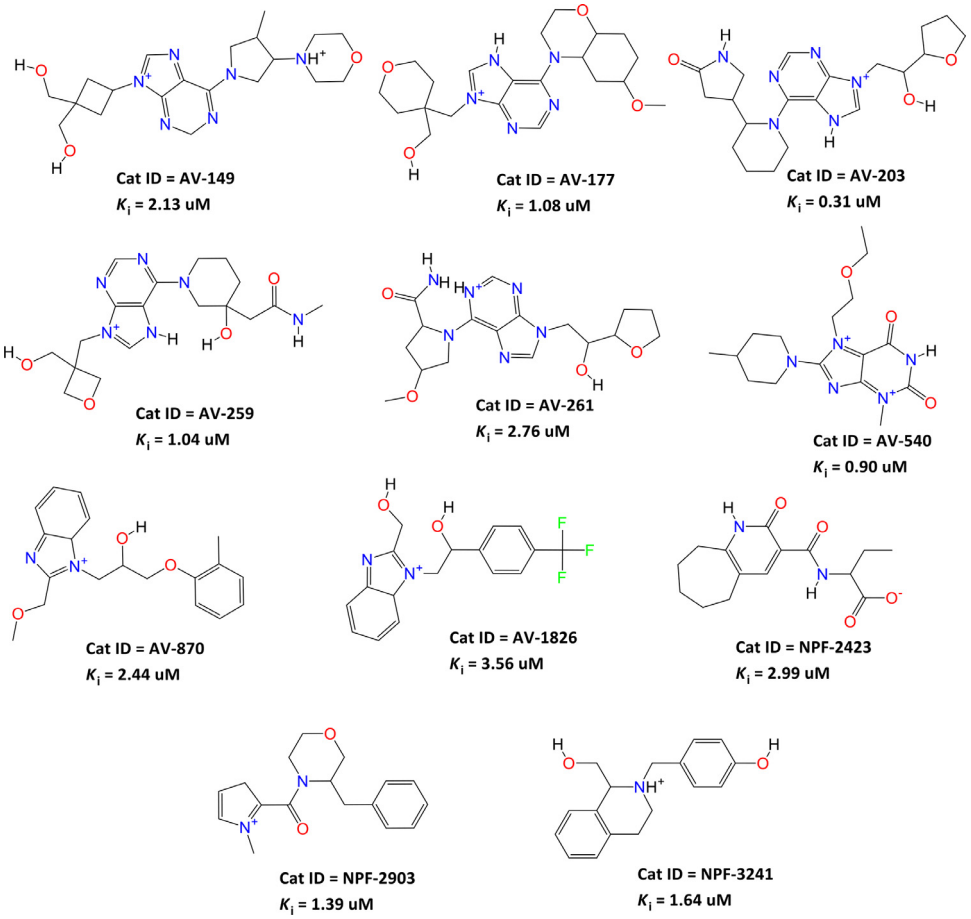

Fig. 2. Chemical structures of the eleven hits as identified by AutoDock4.2 program

used to dock the MOE 32-hits and successful candidates were selected, once more, based on the earlier defined two criteria. AutoDock4.2 program ranked only 12 out of the 32 molecules higher than N3, unlike MOE docking program. Nevertheless, all the compounds were good binders to M^{PRO} with free energy of binding ranging from −5.21 to −8.87 kcal/mol and demonstrated better ligand efficiencies (ranging from 0.22 to 0.39 kcal/mol per non-H atom) than N3 (0.15 kcal/mol per non-H atom) (Table 1). The reasonable ligand efficiencies and excellent physicochemical features of these compounds (molar weight < 400 Da, hydrogen bond acceptor/donor < 7/4, topological polar surface area < 140, number of rotatable bonds < 5, lipophilicity < 4) highlight their significance as interesting starting materials for developing novel corona virus M^{PRO} inhibitors and corona virus drugs. Furthermore, visual inspection of the ligand poses identified that all but one made interactions with the catalytic residues (Cys145 and His41) of the receptor bringing the final number of virtual hits according to our cut-off to 11 compounds, which consist of 3 natural products fragments and 8 antivirals.

Structure-activity relationship (SAR) derived from the eleven hits

Analysis of the chemical structures of the eleven in-silico hit compounds vis-à-vis their theoretical inhibition constants (K_i) revealed they all have certain unprecedented common features which probably are critical for binding interaction with M^{PRO} [12–14]. Firstly, all the eleven compounds were found to contain quaternary N atom(s) except NPF-2423, suggesting that the presence of compounds possessing a positive charge on the atom in the position of the nitrogen could be critical for interaction with the protein. This is consistent with the nature of N3, the cocrystallized inhibitor. However, it does seem that the presence of more than one of this moiety – quaternary N atom - in a compound does not improve potency since the activities of AV-149 (K_i = 2.13 μM) and AV-540 (K_i = 0.90 μM) with two quaternary N atoms are less than that of AV-203 (K_i = 0.31 μM) with single quaternary N atom. Secondly, it was observed that each of the eleven compounds have two carbons separating N and O atoms either in a ring or straight chain arrangement. Thus, it can be hypothesized that the presence of the quaternary nitrogen atom and N atom separated from O atom by not more than two carbon atoms in a compound are necessary feature behind their interactions with the corona virus M^{PRO}. Other functionalities worthy

Table 1
Docking results of AutoDock4.2 program.

Dataset	Binding free energy (kcal/mol)	Inhibition constant (μM)	Ligand efficiency
NPF-1103	−6.90	8.75	0.33
NPF-2110	−7.21	5.22	0.34
NPF-2423	−7.54	2.99	0.36
NPF-2903	−7.99	1.39	0.38
NPF-3241	−7.89	1.64	0.39
NPF-3246	−7.53	3.03	0.36
NPF-3767	−6.81	10.14	0.43
NPF-3801	−7.16	5.65	0.36
AV-2	−6.45	18.71	0.21
AV-48	−5.80	56.30	0.31
AV-122	−7.22	5.12	0.27
AV-149	−7.74	2.13	0.27
AV-151	−6.58	15.15	0.24
177-AV	−8.14	1.08	0.27
AV-187	−7.28	4.61	0.27
AV-202	−7.31	4.35	0.27
AV-203	−8.87	0.31	0.31
AV-215	−6.35	22.13	0.23
AV-224	−6.26	25.59	0.23
AV-253	−5.21	151.73	0.20
AV-259	−8.16	1.04	0.29
AV-261	−7.58	2.76	0.28
AV-270	−6.27	25.31	0.22
AV-540	−8.25	0.90	0.34
AV-850	−6.78	10.75	0.31
AV-870	−7.66	2.44	0.32
AV-1826	−7.43	3.56	0.31
AV-1871	−6.49	17.39	0.27
AV-2077	−6.67	12.91	0.29
AV-2192	−6.10	33.95	0.24
AV-2556	−7.06	6.64	0.34
AV-3893	−6.80	10.29	0.28
N3	−7.40	3.79	0.15

K_i is the theoretical inhibition constant and like binding energy, lower values indicate more favorable interaction. Ligand efficiency is a concept that expresses the sensitivity of binding affinity to an increase in molecular size. The higher the ligand efficiency the better the molecule is as drug-lead [34].

of mention are amide, purine and their pseudo forms. These were present in many of the hits and may have well played pivotal role in ensuring binding interaction.

Analysis of binding poses of the hits

Information obtained from analysis of key molecular interactions formed between potential drug and protein target is essential because it guides synthesis of derivatives in structure-activity optimization exercise [35–36]. To this end, the binding modes of the eleven best performing candidates were determined. Docking calculation on AV-149 (Fig. 3a) identified a unique binding pose in which the hydroxyl group made strong hydrogen bonds with carboxylate moieties of Gly143 and Thr26 backbones. Aside using its hetero-oxygen to make hydrogen bonding with Gln192 and Pro168 side chains, the morpholine group of the compound had an intriguing hydrogen bond contact with the Thr190 and Glu166 backbone carbonyl moieties and Met165 thiol group. The cyclobutyl ring interacted with SH group of Cys145 while His41 had pi-pi contact with the aromatic rings of the ligand. AV-177 (Fig. 3b) accommodated its hydroxyl group within the inner groove of M^{PRO} binding pocket to make hydrogen bonds with Asp187 and Arg188. The morpholine ring had hydrogen bonding interactions with Cys145 SH group and His163 imidazole ring while His41 was found having a pi-pi intercourse with the ligand's purine ring. The most active compound (AV-203) (Fig. 3c) identified in this study adopted a unique binding mode within the binding cavity of M^{PRO}. The compound hydrogen bond with His163 imidazole NH group through its furan oxygen atom. The only hydroxyl moiety of the compound hydrogen bond with His164 carbonyl backbone and Cys145 SH group. Both backbones of Arg188 and Glu166 had hydrogen bonding intercourse with the pyridine nucleus while pyrrolidinone related with the side chain of Ala191. The conformation of the compound must have enabled pi-pi interactions between its purine moiety and the surrounding protein residues with aromatic rings. The best docked conformation of AV-259 (Fig. 3d) revealed a polar contact between purine NH group and SH group of the catalytic residue, Cys145. In addition, piperidinol OH group and the terminal NH group of the compound hydrogen bond with His163 imidazole NH group and Phe140 backbone, respectively. Further interactions were observed with Met49 and Glu166. His41 and His164 imidazole groups were again found making pi-pi interactions with M^{PRO} purine ring. Docking calculations on AV-261 (Fig. 3e) revealed a unique binding conformation

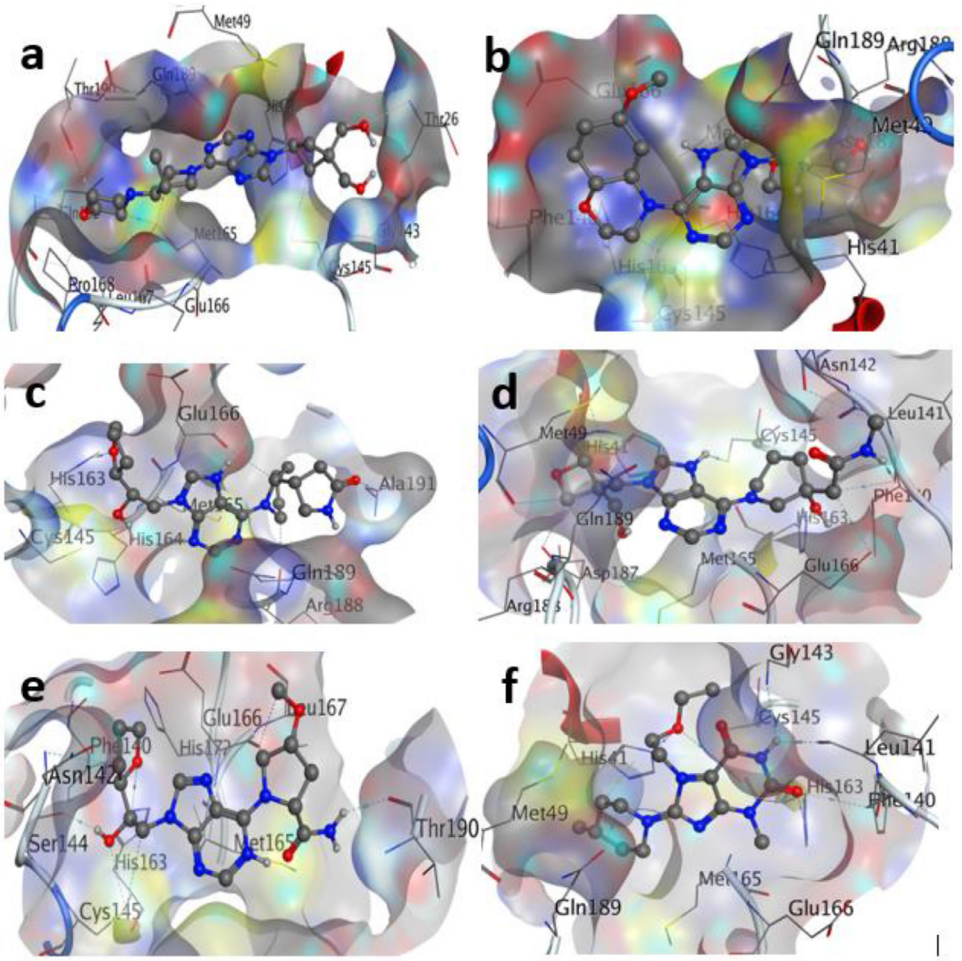

Fig. 3. Theoretical binding poses for the virtual hits. The protein residue are represented in line format while the ligands are shown in ball and stick format. Atoms of the ligands are color coded: gray = carbon, red = oxygen, blue = nitrogen and white = hydrogen. The background represent the protein's molecular surface according to MOE representation. Subfigures a-f respectively show the binding poses of AV-147, AV-177, AV-203, AV-259, AV-261 and AV-540 in SARS-CoV-2 M^{PRO} binding site. Fig. 3. Theoretical binding poses for the virtual hits. The protein residue are represented in line format while the ligands are shown in ball and stick format. Atoms of the ligands are color coded: gray = carbon, red = oxygen, blue = nitrogen and white = hydrogen. The background represent the protein's molecular surface according to MOE representation. Subfigures g-k respectively show the binding poses of AV-870, AV-1826, NPF-2423, NPF-2903 and NPF-3241 in SARS-CoV-2 M^{PRO} binding site.

toward M^{PRO}. The only hydroxyl group of the compound that forms hydrogen bond with SH group of Cys145 and Ser144 side chain. Hydrogen bond contact was found between the furan ring and His163 imidazole NH group. Unlike what has been found so far, the purine nucleus made an arene-hydrogen interaction with Met165. The amide NH group related with Thr190 backbone while the pyrrolidine ring contacted the side chain of Glu166. The binding conformation of the second most active compound (AV-540) (Fig. 3f) in this study had arene-hydrogen interactions with the catalytic dyad (His41 and Cys145). Furthermore, the ethoxyethyl oxygen atom made polar contacts with the SH and imidazole NH groups of Cys145 and His41 respectively. Additionally, the carbonyl groups and ring NH moiety interacted with Gly143, His163, Phe140, and Leu141 of M^{PRO}.

The docked conformation of AV-870 (K_i = 2.44 μM) (Fig. 3g) showed hydophobic force mainly drove the protein-ligand complexation. The ligand stretched in such a way that its two terminal aromatic rings docked into the protein groove surrounded by amino acid residues like Phe140, His163, His172, His41 and Tyr54, which are capable of forming pi-pi interaction through their aromatic rings. The only observable hydrogen bonding contact existed between the hydroxyl moiety and SH group of Cys145. The least theoretical free energy of AV-1826 (K_i = 3.56 μM) showed a docked pose similar to AV-870 (Fig. 3h). Both aromatic rings of the ligand made lipophilic contacts with protein residues listed for AV-870. The supremacy of hydrophobic interactions in the ligand binding is revealed in the fact that the presence of the three fluorine atoms reduced the inhibitory activity, perhaps because the fluorine atoms being highly electronegative molecule distorted the hydrophobic forces, though there are hydrogen bonds between the hydroxyl groups and Cys145, Gly143 and Gln189 residues. The only natural product carbamic acid identified in this study has a docked pose that showed its ethyl chain accommodated

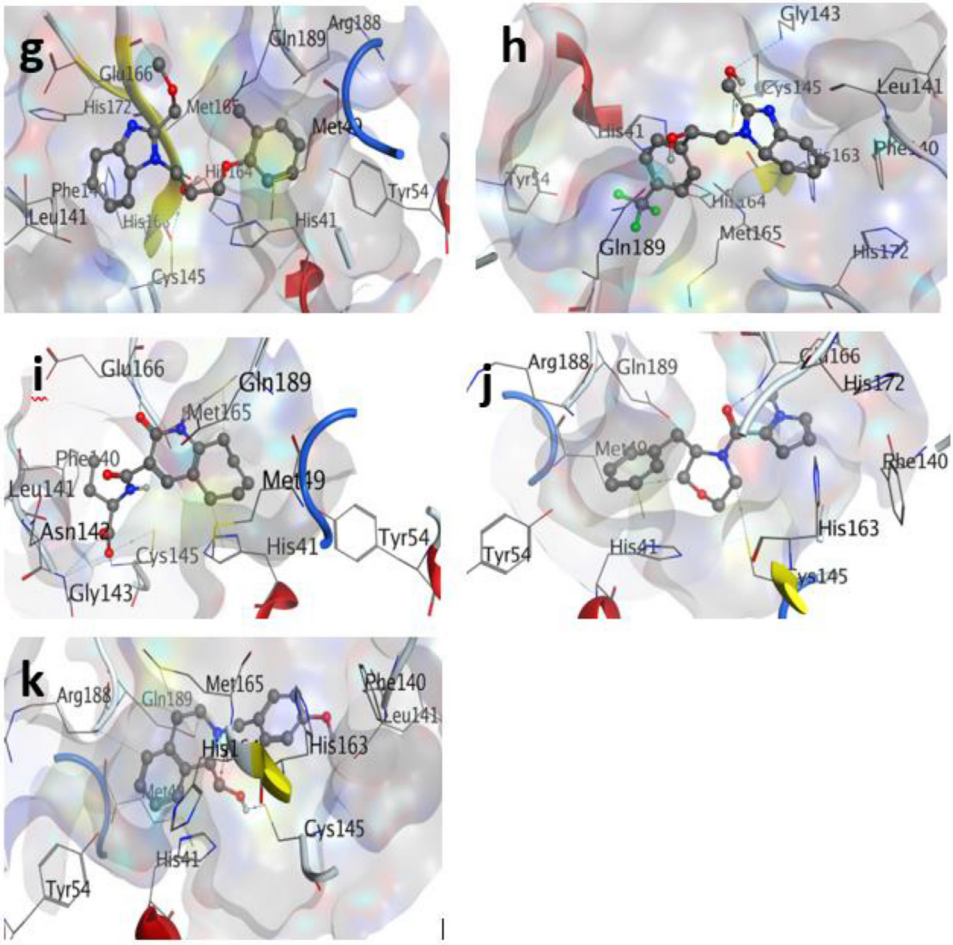

Fig. 3. Continued

in the protein groove surrounded by amino acid residues with hydrophobic side chains (Phe140 and Leu141) (Fig. 3i). The carboxylate group established a hydrogen bond contact with Cys145 SH, Gly143 backbone and Asn142 side chain. The ligand related with the other catalytic residue - His41 – through arene-hydrogen bonding. The pyridinone was found to make two hydrogen bonds with Met165 sulfane group and Glu166 backbone. The smallest sized natural product identified as virtual hit assumed a unique binding mode (Fig. 3j) in which its toluenyl group flanked into the M^{PRO} hydrophobic pocket to make pi-pi contacts with aromatic rings of His41, Tyr54 and His164. Two hydrogen bonds were observed between the morpholine ring and Cys145 SH group and between the carbonyl moiety and Gln189 side chain. Finally, the aromatic rings of NPF-3241 had the usual pi-pi interactions with the usual aromatic rings of the protein residues (Fig. 3k). The two hydroxyl groups of the ligand established hydrogen bonds with Cys145 SH group and Leu141 backbone. Further binding contact was observed between the ligand piperidine moiety and His164 backbone and Gln189 and Met165 side chains.

Stability of the complex M^{pro} with ligands

During the MD simulation in this present study, 50 ns simulation was carried out to ensure that the equilibration phase of ligand-receptor complex lasted long enough to analyze for stable intermolecular interaction. RMSD values of the backbone atoms of the small-molecules (in red color) in comparison with M^{PRO} active site residues (in blue color) of the heating phase were used to assess stability. Only the topmost scoring compound (AV-203) remained stable within the protein binding site at the course of 50 ns MD simulation period. Even though it intermittently moved away a little bit from the protein, for example between 6 and 13 ns and 33 to 45 ns simulation time, overall AV-203 stayed within less than RMSD of 1.0 Å to M^{PRO} active site residues as the complex evolved over the simulation period (Fig. 4). Of the compounds, five flew out of the protein binding site almost as soon as the equilibration began while the other five drifted to distances relatively unfavorable for binding interaction (Figure S1). Taken together, the MD simulation result alongside the reasonable ligand efficiency of

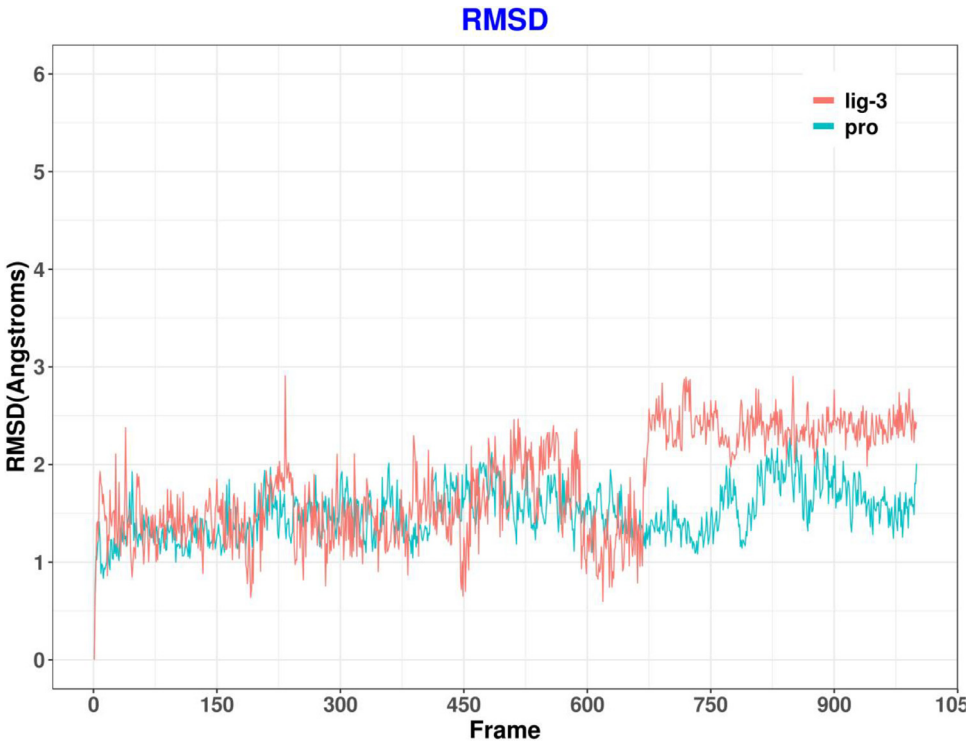

Fig. 4. RMSD values for AV-203 ligand relative to M^{PRO} structure during MD simulation. AV-203 is represented as Lig-3 in red color while M^{PRO} as pro in blue color.

AV-203 (0.31 kcal/mol per number of heavy atoms) suggest that its interaction with the target would last long enough to effect physiological response and hence it qualifies as a suitable template for development of new M^{PRO} inhibitors.

Conclusion

We have virtually screened two datasets, antiviral compounds and natural products fragments from Enamine database, for their ability to interact with a genetically validated SARS-CoV-2 drug target (M^{PRO}) by employing techniques such as: docking and free binding energy calculations, redocking and rescoring, molecular dynamic simulation of protein-ligand complexes of topscorers, analysis of SAR and binding mode predictions. Eleven compounds selected as good binders after ranking and reranking were based on their; ability to exhibit higher binding affinity than the co-crystallized inhibitor and binding contact with the protein catalytic dyad. The result of their SAR suggests that the identified common features among them are important for their interactions with M^{PRO}. Hence, we hope to consider these features in developing a pharmacophore model and determine whether it can distinguish M^{PRO} actives from inactives in our subsequent work. Interesting binding interactions were observed upon analysis of the compound poses. At the end, we considered the topmost scoring compound coded as AV-203 as our virtual hit because it is the only one that demonstrated good binding stability during the period of 50 ns MD simulations. We intend to collaborate with researchers in biological screening field to confirm the inhibitory potency of AV-203 in biological assay.

Declaration of Competing Interest

The authors declare that they have no known competing financial interests or personal relationships that could have appeared to influence the work reported in this paper.

Acknowledgements

Dr Ibezim A. acknowledges the African-German Network of Excellence in Science (AGNES) junior researcher grant supported by Alexander von Humboldt and sponsored by the Federal Ministry of Education and Research. Mr Simoben CV of Martin Lurther University, Halle-Wittenberg, Institute of Pharmacy, Germany is appreciated for his computational support.

Funding statement

This work was supported by the Tertiary Education Trust Fund (TETFund), Nigeria [grant number: TETF/ES/DR&D-CE/NRF2020/SETI/53/VOL.1].

Supplementary materials

Supplementary material associated with this article can be found, in the online version, at doi:10.1016/j.sciaf.2021.e00970.

References

[1] B. Hu, H. Guo, P. Zhou, Z.L. Shi, Characteristics of SARS-CoV-2 and COVID-19, Nat. Rev. Microbiol. 19 (2021) 141–154.
[2] D. Henry, E. Sancelme, A. Finon, E. Esteve, Urticarial eruption in COVID-19 infection, J. Eur. Acad. Dermatol. Venereol. (2020), doi:10.1111/jdv.16472.
[3] K. Andam, H. Edeh, V. Oboh, K. Pauw, J. Thurlow, Impacts of COVID-19 on food systems and poverty in Nigeria, Adv. Food Secur. Sust. 5 (2020) 145–173.
[4] C. Chaccour, F. Hammann, S. Ramon-Garcia, N.R. Rabinovich, Ivermectin and COVID-19: keeping rigor in ties of urgency, Am. J. Trop. Med. Hyg. 102 (2020) 1156–1157.
[5] N.K. Dutta, K. Mazumdar, J.T. Gordy, The nucleocapsid protein of SARS–CoV-2: a target for vaccine development, J. Virol. 94 (2020) e00647–e00720, doi:10.1128/JVI.00647-20.
[6] A. Sternberg, C. Naujokat, Structural features of coronavirus SARS-CoV-2 spike protein: targets for vaccination, Life Sci. 257 (2020) 118–156.
[7] D. Schoeman, B.C. Fielding, Coronavirus envelope protein: curent knowledge, Virol J (2019), doi:10.1186/s12985-019-1182-0.
[8] M.I. Artika, A.K. Dewantari, Wiyatno, Molecular biology of coronaviruses: current knowledge, Heliyon 6 (2020) e04743.
[9] O.O. Olubiyi, M. Olagunju, M. Keutman, J. Loschwitz, B. Strodel, High throughput virtual screening to discover inhibitors of the main protease of the coronavirus SARS-CoV-2, Molecules (2020), doi:10.3390/molecules25143193.
[10] S. Illrich, C. Nitsche, The SARS-CoV-2 main protease as drug target, Bioorg. Med. Chem. Lett. 30 (2020) 127–137.
[11] Z. Jin, X. Du, Y. Xu, Y. Deng, M. Liu, Y. Zhao, B. Zhang, X. Li, L. Zhang, C. Peng, Y. Duan, J. Yu, L. Wang, K. Yang, F. Lius, R. Jiang, X. Yang, T. You, X. Lius, X. Yang, F. Bai, H. Liu, X. Liu, L.W. Guddat, W. Xu, G. Xiao, C. Qin, Z. Shi, H. Jiang, Z. Rao, H. Yang, Structure of Mpro from SARS-CoV-2 and discovery of its inhibitors, Nature 582 (2020) 289–293.
[12] R. Ghosh, A. Chakraborty, A. Biswas, S. Chowdhuri, Depicting the inhibitory potential of polyphenols from Isatis indigotica root against the main protease of SARS CoV-2 using computational approaches, J. Biomol. Struct. Dyn. 9 (2020) 1–12.
[13] K.A. Peele, C.P. Durthi, T. Srihansa, S. Krupanidhi, A.V. Sai, D.J. Babu, M. Indira, A.R. Reddy, T.C. Venkateswarulu, Molecular docking and dynamic simulations for antiviral compounds against SARS-CoV-2: a computational study, Inf. Med. Unlocked (2020), doi:10.1016/j.imu.2020.100345.
[14] S. Kumar, P.P. Sharma, U. Shankar, D. Kumar, S.K. Joshi, L. Pena, R. Durvasula, A. Kumar, P. Kempaiah, A.B. Rathi, Discovery of new hydroxyethylamine analogs against $3CL^{pro}$ protein target of SARS-COV-2: molecular docking, molecular dynamics simulation and structure-activity relationship studies, J. Chem. Inf. Model. (2020), doi:10.1021/acs.jcim.0c00326.
[15] M.T. Khan, A. Ali, Q. Wang, M. Irfan, A. Khan, M.T. Zeb, Y. Zhang, S. Chinnasamy, D. Wei, Marine natural compounds as potents inhibitors against the main protease of SARS-CoV-2. A molecular dynamic study, J. Biomol. Str. Dyn. (2020), doi:10.1080/07391102.2020.1769733.
[16] M.A.A. Ibrahim, A.H.M. Abdelrahman, T.A. Hussien, E.A.A. Badr, T.A. Mohamed, H.R. El-Seedi, P.W. Pare, T. Efferth, M.F. Hegazy, In silico drug discovery of major metabolites from spices as SARS-CoV-2 main protease inhibitors, Comput. Biol. Med. 126 (2020) 104046, doi:10.1016/j.compbiomed.2020.104046.
[17] M.A.A. Ibrahim, A.H.M. Abdelrahman, K.S. Allemailem, A. Almatroudi, M.F. Moustafa, M.F. Hegazy, In silico evaluation of prospective anti-COVID-19 drug candidates as potential SARS-CoV-2 main protease inhibitors, Protein J. 2 (2020) 1–14, doi:10.1007/s10930-020-09945-6.
[18] M.A.A. Ibrahim, K.A.A. Abdeljawaad, A.H.M. Abdelrahman, M.E.F. Hegazy, Natural-like products as potential SARS-CoV-2 Mpro inhibitors: in-silico drug discovery, J. Biomol. Str. Dyn. (2020), doi:10.1080/07391102.2020.1790037.
[19] M.A.A. Ibrahim, A.H.M. Abdelrahman, M.E.F. Hegazy, In-silico drug repurposing and molecular dynamics puzzled out potential SARS-CoV-2 main protease inhibitors, J. Biomol. Str. Dyn. (2020), doi:10.1080/07391102.2020.1791958.
[20] M.A.A. Ibrahim, E.A.R. Mohamed, A.H.M. Abdelrahman, K.S. Allemailem, M.F. Moustafa, A.M. Shawky, A. Mahzari, A.R. Hakami, K.A.A. Abdeljawaad, M.A.M. Atia, Rutin and flavone analogs as prospective SARS-CoV-2 main protease inhibitors: in silico drug discovery study, J. Mol. Graphics Model. 105 (2021) 1079042.
[21] A. Ibezim, B. Debnath, F. Ntie-Kang, C.J. Mbah, N.J. Nwodo, Binding of anti-Trypanosoma natural products from African flora against selected drug targets: a docking study, Med. Chem. Res. 26 (2017) 562–579.
[22] F. Ntie-Kang, N.J. Nwodo, A. Ibezim, C.V. Simoben, B. Karaman, V.F. Ngwa, W. Sippl, M.U. Adikwu, M.L. Mbaze, Molecular modeling of potential anti-cancer agents from African medicinal plants, J. Chem. Inf. Model. 54 (2014) 2433–2450.
[23] A. Ibezim, E.A. Onoabedje, I.C. Adaka, K.O. Omeje, U.S. Onoabedje, B.C. Obi, Carboxamides bearing sulfonamide functionality as potential novel phospholipase a_2 inhibitors, Chemistryselect (2020), doi:10.1002/slct.202003784.
[24] G.M. Morris, D.S. Goodsell, R.S. Halliday, R. Huey, W.E. Hart, R.K. Belew, Automated docking using a lamarckian genetic algorithm and an empirical binding free energy function, J. Comp. Chem. 19 (1998) 1639–1662.
[25] Malde Ak, L. Zuo, M. Breeze, M. Stroet, D. Poger, P.C. Nair, C. Oostenbrink, A.E. Mark, An Automated force field Topology Builder (ATB) and repository: version 1.0, J. Chem. Theory Comput. 7 (2011) 4026–4037.
[26] A. Ibezim, B.C. Obi, N.M. Ofokansi, C.J. Mbah, N.J. Nwodo, Discovery of trypanocidal bioactive leads by docking study, molecular dynamic simulation and in vivo screening, ChemistrySelect 3 (2018) 2386–2389.
[27] A. Ibezim, B. Debnath, F. Ntie-Kang, C.J. Mbah, N.J. Nwodo, Binding of anti-Trypanosoma natural products from African flora against selected drug targets: a docking study, Med. Chem. Res. 26 (2017) 562–579.
[28] N.J. Nwodo, A. Ibezim, F. Ntie-Kang, M.U. Adikwu, C.J. Mbah, Anti-Trypanosomal activity of Nigerian plants and their constituents, Molecules 20 (2015) 7750–7771.
[29] A. Ibezim, O.O. Olujide, K. Ata, C.J. Mbah, N.J. Nwodo, Structure-based study of natural products with anti-Schistoma activity, Curr. Comp. Aided Drug Des. 13 (2017) 91–100.
[30] N.J. Nwodo, A. Ibezim, F. Ntie-Kang, M.U. Adikwu, C.J. Mbah, Anti-trypanosomal activity of Nigerian plants and their constituents, Molecules 20 (2015) 7750–7771.
[31] L. Lin, W. Hsu, C. Lin, Antiviral natural products and herbal medicines, J. Trad. Compl. Med. 4 (2014) 24–35.
[32] M.T. Islam, C. Sarkar, D.M. El-Kersh, S. Jamaddar, S.J. Uddin, J.A. Shilpi, M.S. Mubarak, Natural products and their derivatives against coronavirus: a review of the non-clinical and pre-clinical data, Pytother. Res. (2020), doi:10.1002/ptr.6700.
[33] D.J. Newman, G.M. Cragg, Natural products as sources of new drugs over the 30 years from 1981 to 2010, J. Nat. Prod. 75 (2010) 311–335.
[34] P.W. Kenny, The nature of ligand efficiency, J. Cheminf. 11 (2019) 8 doi.10.1186/s13321-019-0330-2.
[35] E.A. Onoabedje, A. Ibezim, U.C. Okoro, S. Batra, Synthesis, molecular docking, antiplasmodial and antioxidant activities of new sulfonamido-pepetide derivatives, Heliyon (2020), doi:10.1016/j.heliyon.2020.e04958.
[36] D.I. Ugwu, U.C. Okoro, P.O. Ukoha, S. Okafor, A. Ibezim, N.M. Kumar, Synthesis, characterization, molecular docking and in vitro antimalarial properties of new carboxamides bearing sulphonamide, Eur. J. Med. Chem. 135 (2017) 349–369.